# A new volcanic province: an inventory of subglacial volcanoes in West Antarctica

MAXIMILLIAN VAN WYK DE VRIES*, ROBERT G. BINGHAM & ANDREW S. HEIN

*School of GeoSciences, University of Edinburgh, Drummond Street, Edinburgh EH8 9XP, UK*

*Correspondence: gmaxvwdv@gmail.com*

**Abstract:** The West Antarctic Ice Sheet overlies the West Antarctic Rift System about which, due to the comprehensive ice cover, we have only limited and sporadic knowledge of volcanic activity and its extent. Improving our understanding of subglacial volcanic activity across the province is important both for helping to constrain how volcanism and rifting may have influenced ice-sheet growth and decay over previous glacial cycles, and in light of concerns over whether enhanced geothermal heat fluxes and subglacial melting may contribute to instability of the West Antarctic Ice Sheet. Here, we use ice-sheet bed-elevation data to locate individual conical edifices protruding upwards into the ice across West Antarctica, and we propose that these edifices represent subglacial volcanoes. We used aeromagnetic, aerogravity, satellite imagery and databases of confirmed volcanoes to support this interpretation. The overall result presented here constitutes a first inventory of West Antarctica's subglacial volcanism. We identified 138 volcanoes, 91 of which have not previously been identified, and which are widely distributed throughout the deep basins of West Antarctica, but are especially concentrated and orientated along the >3000 km central axis of the West Antarctic Rift System.

West Antarctica hosts one of the most extensive regions of stretched continental crust on the Earth, comparable in dimensions and setting to the East African Rift System and the western USA's Basin and Range Province (Fig. 1) (e.g. see Behrendt *et al.* 1991; Dalziel 2006; Kalberg *et al.* 2015). Improved knowledge of the region's geological structure is important because it provides the template over which the West Antarctic Ice Sheet (WAIS) has waxed and waned over multiple glaciations (Naish *et al.* 2009; Pollard & DeConto 2009; Jamieson *et al.* 2010), and this provides a first-order control on the spatial configuration of the WAIS' ice dynamics (Studinger *et al.* 2001; Jordan *et al.* 2010, Bingham *et al.* 2012). The subglacial region today is characterized by an extensive and complex network of rifts, which is likely to have initiated at various times since the Cenozoic (Fitzgerald 2002; Dalziel 2006; Siddoway 2008; Spiegel *et al.* 2016), and which in some locations may still be active (Behrendt, *et al.* 1998; LeMasurier 2008; Lough *et al.* 2013; Schroeder *et al.* 2014). Collectively, this series of rifts beneath the WAIS has been termed the West Antarctic Rift System (WARS), and is bounded by the Transantarctic Mountains to the south (Fig. 1).

In other major rift systems of the world, rift interiors with thin, stretched crust are associated with considerable volcanism (e.g. Siebert & Simkin 2002). However, in West Antarctica, only a few studies have identified subglacial volcanoes and/or volcanic activity (e.g. Blankenship *et al.* 1993; Behrendt *et al.* 1998, 2002; Corr & Vaughan 2008; Lough *et al.* 2013), with the ice cover having deterred a comprehensive identification of the full spread of volcanoes throughout the WARS. Improving on this limited impression of the WARS' distribution of volcanism is important for several reasons. Firstly, characterizing the geographical spread of volcanic activity across the WARS can complement wider efforts to understand the main controls on rift volcanism throughout the globe (Ellis & King 1991; Ebinger *et al.* 2010). Secondly, volcanic edifices, by forming 'protuberances' at the subglacial interface, contribute towards the macroscale roughness of ice-sheet beds, which in turn forms a first-order influence on ice flow (cf. Bingham & Siegert 2009). Thirdly, volcanism affects geothermal heat flow and, hence, basal melting, potentially also impacting upon ice dynamics (Blankenship *et al.* 1993; Vogel *et al.* 2006). Fourthly, it has been argued that subglacial volcanic sequences can be used to recover palaeoenvironmental information from Quaternary glaciations, such as palaeo-ice thickness and thermal regime (e.g. Smellie 2008; Smellie & Edwards 2016).

In this contribution, we present a new regional-scale assessment of the likely locations of volcanoes in West Antarctica based on a morphometric (or shape) analysis of West Antarctica's ice-bed topography. Volcano shape depends on three principal factors: (1) the composition of the magma
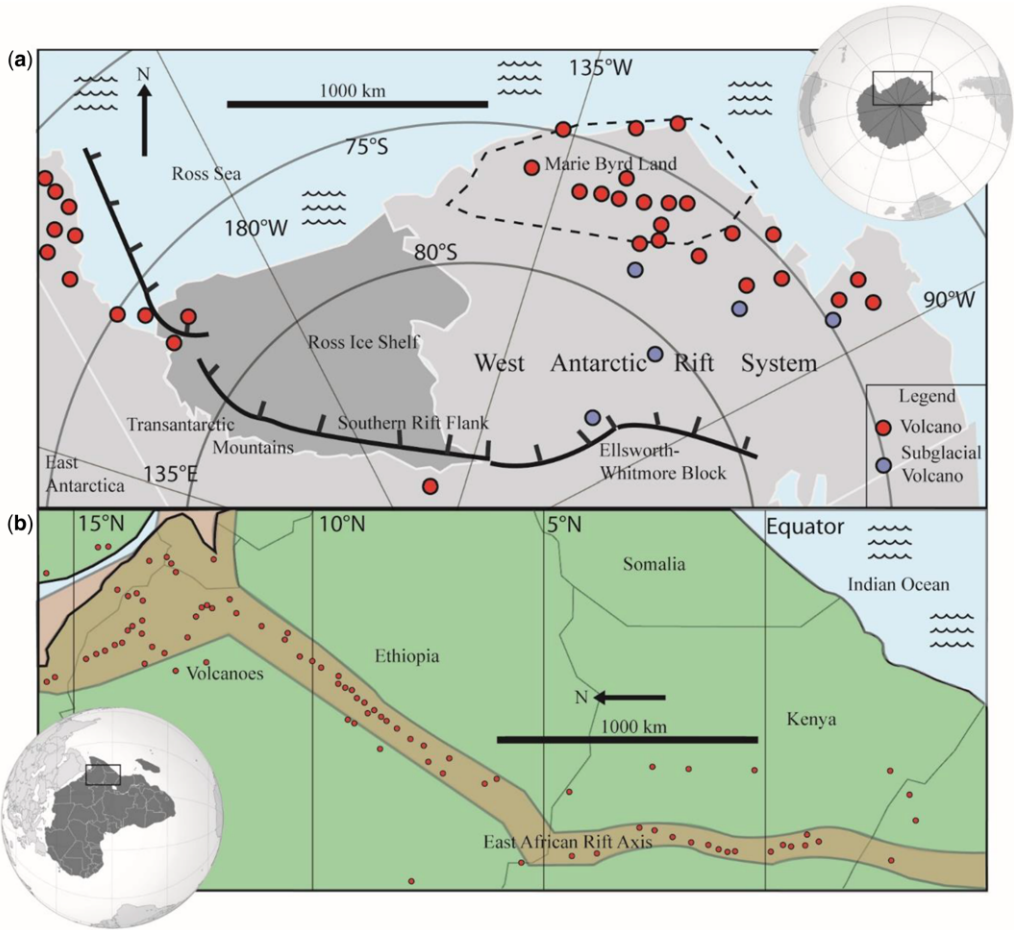
**Fig. 1.** (**a**) Location of the main components of the West Antarctic Rift System and confirmed volcanoes (red circles: after LeMasurier *et al.* 1990; Smellie & Edwards 2016). (**b**) Location of Holocene volcanoes (red circles) in the Ethiopia/Kenya branch of the East African Rift (red shaded area). The majority of this activity is aligned along the rift axis with occasional flank volcanism. Data from Siebert & Simkin (2002) and Global Volcanism Program (2013).

erupted; (2) the environment into which the magma has been erupted; and (3) the erosional regime to which the volcano has been subjected since eruption (Hickson 2000; Grosse *et al.* 2014; Pedersen & Grosse 2014). Magma composition in large continental rifts generally has low–medium silica content with some more alkaline eruptions (Ebinger *et al.* 2013). In West Antarctica, where most knowledge of volcanoes is derived from subaerial outcrops in Marie Byrd Land, volcanoes are composed of intermediate alkaline lavas erupted onto a basaltic shield, with smaller instances being composed entirely of basalt and a few more evolved compositions (trachyte, rhyolite: LeMasurier *et al.* 1990; LeMasurier 2013). We therefore consider it likely that many structures in the WARS are also basaltic. Regarding the environment of eruption, subaerial basaltic

eruptions typically produce broad shield-type cones protruding upwards from the surrounding landscape (Grosse *et al.* 2014). Under subglacial conditions, monogenetic volcanoes often form steeper-sided, flat-topped structures made up of phreatomagmatic deposits draped on pillow lava cores and overlain by lava-fed deltas known as tuyas (Hickson 2000; Pedersen & Grosse 2014; Smellie & Edwards 2016). Larger, polygenetic volcanic structures give rise to a range of morphometries reflecting the multiple events that cause their formation, but many also have overall 'conical' structures similar to stratovolcanoes or shield volcanoes (Grosse *et al.* 2014; Smellie & Edwards 2016).

In the WARS, the macrogeomorphology is dominated by elongate landforms resulting from geological rifting and subglacial erosion. We

propose here that, in this setting, the most reasonable explanation for any 'cones' being present is that they must be volcanic in origin. We define 'cones' as any features that have a low length/width ratio viewed from above; hence, for this study, we include cones even with very low slope angles. Thus, we use cones in this subglacial landscape as diagnostic of the presence of volcanoes. We note that identifying cones alone will by no means identify all volcanism in the WARS. For example, volcanic fissures eruptions, a likely feature of rift volcanism, will yield ridge forms, or 'tindars' (Smellie & Edwards 2016), rather than cones. Moreover, in the wet basal environment of the WAIS, the older the cone the more likely it will have lost its conical form from subglacial erosion. Therefore, cones present today are likely to be relatively young – although we cannot use our method to distinguish whether or not the features are volcanically active.

## Methods

Our underpinning methodology was to identify cones that protrude upwards from a digital elevation model (DEM) of Antarctica's subglacial topography, and to assess the likelihood that each cone is a volcanic edifice. We undertook our analysis on the Bedmap2 DEM (Fretwell *et al.* 2013) domain encompassed by the WARS, which incorporates all of West Antarctica, the Ross Ice Shelf and the Transantarctic Mountains fringing East Antarctica that flank the WARS (Elliott 2013). Importantly, while Bedmap2 represents the state-of-the-art knowledge of West Antarctica's subglacial landscape, it is derived from variable data coverage, the vast majority of the data being sourced from airborne radar-sounding acquired along one-dimensional tracks. Along the radar tracks the horizontal spacing of bed-elevation data points can reach a few metres, but between tracks the spacing is often several kilometres. The DEM itself is presented as a 1 km gridded product, although the raw data were initially gridded at 5 km (Fretwell *et al.* 2013). Therefore, while the DEM cannot capture the fine-scale topography now routinely acquired by satellite and airborne altimetry, and which has been exploited for multiple morphometric analyses (e.g. Pedersen & Grosse 2014; Lindback & Pettersson 2015; Ely *et al.* 2016), it nevertheless presents a workable starting point for identifying volcanic edifices. We consider how some of the DEM's limitations can be overcome in our analysis below.

We defined a cone as an upwards protuberance from the DEM whose elongation ratio (width v. length) <1.5. Over the domain, but excluding non-grounded ice (primarily the Ross Ice Shelf) where the subglacial topography is poorly characterized,

we first extracted cones protruding at least 100 m from the surrounding terrain. The bed-elevation uncertainties within the DEM prevent reliable identification of smaller edifices. Elevation profiles across each cone were then extracted from Bedmap2 at multiple angles with respect to the current ice-flow direction (taken from Rignot *et al.* 2011). Where radar profiles directly traversed a cone, we further cross-checked the shape of the bed directly from the raw data. This is part of our procedure for accounting for any artefacts in Bedmap2, which involves corroborating our identified volcanoes with auxiliary datasets. To assess the likelihood that the Bedmap2-extracted cones were (a) not merely interpolation-induced artefacts and (b) likely represent volcanoes, we implemented a scheme wherein points were awarded where auxiliary data ground-truthed the bed DEM and/or gave greater confidence in a volcanic interpretation. The assessment criteria are as follows, with points awarded for each and data-source references given in Table 1:

(1) Whether a cone is found within 5 km of the nearest raw ice-thickness data.

(2) Whether a cone is overlain by an upwards-protruding prominence in the surface of the ice draped over it. This criterion takes advantage of the fact that, under the right balance between ice thickness and ice-flow speed, subglacial topographical prominences can be expressed at the ice surface (e.g. De Rydt *et al.* 2013).

(3) Whether a cone is discernible as a feature at the ice surface in visible satellite imagery. Various recent studies have demonstrated that subglacial features can be outlined by visible expressions in surface imagery (e.g. Ross *et al.* 2014; Chang *et al.* 2015; Jamieson *et al.* 2016).

(4) Whether a cone is associated with a clear concentric magnetic anomaly. This depends on the potential volcano having a pillow-lava core, rather than being composed solely of tuff. This is consistent with the thickness of ice overlying the cones and the erodibility of tuff/tephra deposits. Strong geomagnetic anomalies have long been suggested as evidence of subglacial volcanism in the WARS (e.g. Behrendt *et al.* 1998, 2002).

(5) Whether a cone is associated with a concentric free-air and/or Bouguer anomaly.

Each cone was assigned a final confidence factor value of between 0 and 5 by summing up the points from the five indicators described above (Table 1).

## Results

Our morphometric analysis of subglacial West Antarctica recovers a total of 178 conical structures

**Table 1.** *Classification scheme used in assessing confidence that a cone extracted from Bedmap2 (Fretwell* et al. *2013) can be interpreted as a volcano*

| Confidence assessment criterion | Dataset/source | Confidence score | | |
| --- | --- | --- | --- | --- |
| | | 0 | 0.5 | 1 |
| (1) Distance to nearest raw ice-thickness measurement | Figure 3 in Fretwell *et al.* (2013) | >15 km | 5–15 km | <5 km |
| (2) Expression in ice-surface DEM overlying identified subglacial cone | Bedmap2 ice-surface DEM: Fretwell *et al.* (2013) | No expression | Associated but off-centre anomaly | Direct overlying anomaly |
| (3) Expression in MODIS imagery of the ice surface overlying the identified subglacial cone | MODIS Mosaic of Antarctica: Scambos *et al.* (2007) | No expression | Weak expression | Clear expression |
| (4) Magnetic anomaly data | ADMAP: Kim *et al.* (2007) | No anomaly | Weak anomaly | Clear anomaly |
| (5) Gravity anomaly data | Studinger *et al.* (2002); Damiani *et al.* (2014); Scheinert *et al.* (2016) | No anomaly | Weak anomaly | Clear anomaly |

Full scores are given in Table 2.

located beneath the grounded WAIS and along the WARS (Fig. 2; Table 2). Of these, 80% are located within 15 km of the raw ice-thickness data measurements (Fretwell *et al.* 2013) and 30% are identified from the DEM at sites where volcanoes, either active or inactive, have previously been identified (LeMasurier *et al.* 1990; LeMasurier 2013; Wardell *et al.* 2014). Many cones were crossed directly by radio-echo-sounding flightlines, allowing verification of their profiles (e.g. Fig. 3) – thus, while there is, inevitably, some smoothing in the Bedmap2 interpolation, the major features of interest are largely captured. One of our confidence tests for volcanic interpretation of cones also takes into account proximity to the raw ice-thickness measurements, further discounting DEM interpolation as a disproportionate influence on the results.

The identified cones range in height between 100 and 3850 m, with an average relief of 621 m, including 29 structures >1 km tall that are mainly situated in Marie Byrd Land and the central rift zone. The basal diameter of the cones ranges between 4.5 and 58.5 km, with an average diameter of 21.3 km. Most of the cones have good basal symmetry, with 63% of the long to short axis ratios being <1.2. Table 3 presents a more in-depth statistical analysis of the morphology of these features and compares them to a global volcanic database (Grosse *et al.* 2014). Figure 4 shows 1:1 cross-sections of three of the newly identified cones along with three prominent shield volcanoes for comparison.

Seventy-eight per cent of the cones achieve a confidence score (from our five-point scheme) >3, and we therefore consider it reasonable to interpret these 138 cones henceforth as subglacial volcanoes. (We note that 98% of the 47 previously identified volcanoes in West Antarctica (visible at the surface and listed by LeMasurier *et al.* 1990) achieved a confidence score >3.) The volcanoes are distributed across subglacial West Antarctica, but are especially concentrated in Marie Byrd Land (one cone per 11 $200 \pm 600$ km$^2$); and along a central belt roughly corresponding to the rift's central sinuous ridge (Behrendt *et al.* 1998), with one cone per $7800 \pm 400$ km$^2$. For comparison, the overall volcanic edifice concentration along the East African Rift is roughly one volcano per 7200 km$^2$, rising to one volcano per 2000 km$^2$ in the densest regions (Global Volcanism Program 2013).

## Discussion

### Morphometry as a tool for identifying subglacial volcanoes

We consider here three main implications that arise from our findings. Firstly, our approach demonstrates that it is possible to use morphometry on Antarctica's subglacial DEM, crucially together with relevant auxiliary information, to identify potential subglacial volcanic edifices beneath West Antarctica. Secondly, it highlights that subglacial West Antarctica – and, in essence, the WARS – comprises one of the world's largest volcanic provinces (cf. LeMasurier *et al.* 1990; Smellie & Edwards 2016), and it provides basic metrics concerning the locations and dimensions of the main volcanic zones. Thirdly, it serves to highlight the wide spread of subglacial volcanism beneath the WAIS, which may impact upon its response to external forcing through affecting coupling of the ice to its bed, and may have implications for future volcanic activity as ice cover thins.

To our knowledge, our study here is the first to use morphometry to identify volcanic edifices on the continental scale beneath Antarctica. The extent of this volcanism has only previously been inferred from geophysical studies (Behrendt *et al.* 2002). Morphometry has been used widely elsewhere in volcanology: for example, to catalogue volcanic parameters, such as height, base width and crater width (e.g. McKnight & Williams 1997; Pedersen & Grosse 2014), or to reconstruct eroded volcanic edifices (Favalli *et al.* 2014). It has been applied to resolve volcanic characteristics in subaerial, submarine (e.g. Stretch *et al.* 2006) and extraterrestrial (e.g. Broz *et al.* 2015) settings. However, in all such cases volcanic morphometry has been applied to DEMs assembled from evenly distributed elevation measurements derived from sensors viewing unobscured surfaces. For subglacial Antarctica, having confidence that the subglacial DEM that has been constructed from non-random elevation measurements has sufficient resolution for the applied interpretation is key. Recent years have witnessed increasing glaciological recovery of subglacial information from morphometry. For example, seeding centres for glaciation of the WAIS (Ross *et al.* 2014) and the East Antarctic Ice Sheet (Bo *et al.* 2009; Rose *et al.* 2013) have been identified by the preponderance of sharp peaks, cirque-like features and closely spaced valleys relative to other parts of the subglacial landscape. Elsewhere, landscapes of 'selective linear erosion', diagnostic of former dynamism in now-stable regions of ice, have been detected from the presence of significant linear incisions (troughs) into otherwise flat higher surfaces (plateaux) (Young *et al.* 2011; Jamieson *et al.* 2014; Rose *et al.* 2014). All of these studies have in common that they have closely considered auxiliary evidence to the morphometry and, hence, have not relied on the surface shape alone in coming to interpretations concerning landscape formation. We have shown here that such a combined approach is also valid for locating and mapping numerous previously
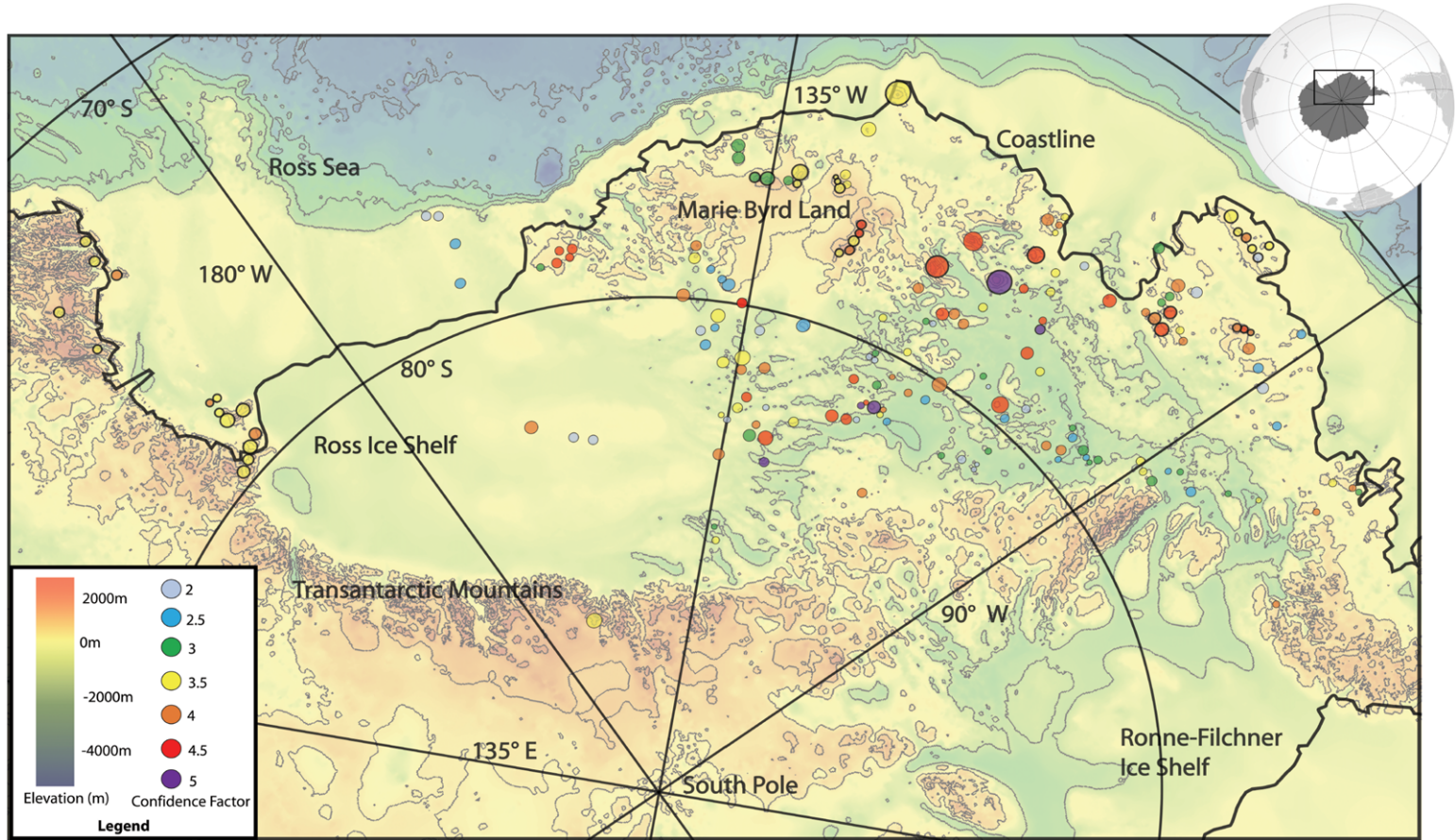
**Fig. 2.** Location map of conical edifices (circles) identified from Bedmap2 (greyscale background) across the West Antarctic Rift System. The data are tabulated in Table 2. The circle colour represents the confidence factor used to assess the likelihood of cones being subglacial volcanoes, and the circle size is proportional to the cone's basal diameter. Circles with black rims represent volcanoes that have been confirmed in other studies (LeMasurier *et al.* 1990; Smellie & Edwards 2016), generally those that have tips which protrude above the ice surface.

**Table 2.** *Tabulation of subglacial cone coordinates, dimensions and volcanic-interpretation confidence factors (see Table 1)*

| Number | Height (m) | Average diameter (km) | Elongation ratio | Volume (km$^3$) | Latitude | Longitude | Volcano confidence factor | | | | | | Previously identified |
|---|---|---|---|---|---|---|---|---|---|---|---|---|---|
| | | | | | | | 1 | 2 | 3 | 4 | 5 | Sum | |
| 1 | 800 | 26 | 1.08 | 106 | −74.00 | −80.38 | 0.5 | 1 | 1 | 0.5 | 0.5 | 3.5 | Yes |
| 2 | 600 | 14 | 1.15 | 23 | −75.60 | −81.60 | 1 | 1 | 0 | 1 | 0.5 | 3.5 | No |
| 3 | 300 | 7.5 | 1.14 | 3 | −76.13 | −83.53 | 1 | 0.5 | 0 | 1 | 0.5 | 3 | No |
| 4 | 300 | 18.5 | 1.18 | 20 | −76.80 | −85.27 | 1 | 0 | 0 | 1 | 0.5 | 2.5 | No |
| 5 | 650 | 24.5 | 1.04 | 77 | −74.47 | −86.40 | 0.5 | 0.5 | 0.5 | 0.5 | 0.5 | 2.5 | No |
| 6 | 350 | 17.5 | 1.19 | 21 | −76.74 | −87.50 | 1 | 0 | 0.5 | 1 | 0.5 | 3 | No |
| 7 | 250 | 17 | 1.27 | 14 | −76.97 | −87.89 | 1 | 0 | 0 | 1 | 0.5 | 2.5 | No |
| 8 | 950 | 29 | 1.07 | 157 | −77.37 | −88.10 | 1 | 0 | 1 | 0.5 | 0.5 | 3 | No |
| 9 | 300 | 19.5 | 1.05 | 22 | −77.40 | −89.38 | 1 | 0.5 | 1 | 0.5 | 0.5 | 3.5 | No |
| 10 | 350 | 15.5 | 1.07 | 17 | −77.32 | −90.34 | 1 | 0.5 | 1 | 0.5 | 0.5 | 3.5 | No |
| 11 | 600 | 32.5 | 1.17 | 124 | −74.27 | −89.58 | 0.5 | 0.5 | 0 | 0.5 | 0.5 | 2 | No |
| 12 | 550 | 36 | 1.06 | 140 | −74.07 | −91.18 | 0.5 | 0 | 1 | 0.5 | 0.5 | 2.5 | No |
| 13 | 450 | 27.5 | 1.20 | 67 | −72.90 | −91.30 | 0 | 1 | 0.5 | 0.5 | 0.5 | 2.5 | No |
| 14 | 500 | 22.5 | 1.25 | 50 | −74.05 | −92.90 | 1 | 1 | 0.5 | 1 | 0.5 | 4 | No |
| 15 | 1400 | 22.5 | 1.25 | 139 | −73.73 | −93.68 | 0.5 | 1 | 1 | 1 | 0.5 | 4 | Yes |
| 16 | 1450 | 19.5 | 1.29 | 108 | −70.03 | −125.97 | 1 | 1 | 1 | 1 | 0.5 | 4.5 | Yes |
| 17 | 1300 | 27 | 1.25 | 186 | −73.89 | −94.64 | 0.5 | 1 | 1 | 1 | 0.5 | 4 | Yes |
| 18 | 400 | 20 | 1.11 | 31 | −78.03 | −92.95 | 1 | 1 | 0 | 0.5 | 0.5 | 3 | No |
| 19 | 325 | 18.5 | 1.18 | 22 | −78.21 | −93.20 | 1 | 1 | 0 | 0.5 | 0.5 | 3 | No |
| 20 | 200 | 9.5 | 1.11 | 4 | −78.20 | −93.82 | 1 | 0.5 | 0 | 0.5 | 0.5 | 2.5 | No |
| 21 | 600 | 20.5 | 1.16 | 49 | −78.15 | −94.62 | 1 | 1 | 0 | 0.5 | 0.5 | 3 | No |
| 22 | 375 | 18.5 | 1.06 | 25 | −78.68 | −95.65 | 1 | 0 | 0.5 | 0.5 | 0.5 | 2.5 | No |
| 23 | 250 | 19 | 1.11 | 18 | −78.52 | −96.16 | 1 | 0.5 | 1 | 1 | 0.5 | 4 | No |
| 24 | 700 | 26.5 | 1.30 | 96 | −78.13 | −96.36 | 1 | 0.5 | 0 | 0.5 | 0.5 | 2.5 | No |
| 25 | 450 | 22.5 | 1.25 | 45 | −78.00 | −97.16 | 1 | 1 | 0 | 0.5 | 0.5 | 3 | No |
| 26 | 250 | 13.5 | 1.25 | 9 | −78.67 | −97.68 | 1 | 1 | 0 | 1 | 1 | 4 | No |
| 27 | 500 | 24.5 | 1.13 | 59 | −74.97 | −96.54 | 0.5 | 1 | 1 | 1 | 0.5 | 4 | No |
| 28 | 400 | 16.5 | 1.36 | 21 | −74.86 | −97.42 | 1 | 1 | 0 | 1 | 0.5 | 3.5 | No |
| 29 | 550 | 16 | 1.13 | 28 | −75.07 | −99.54 | 1 | 1 | 1 | 1 | 0.5 | 4.5 | Yes |
| 30 | 820 | 20.5 | 1.16 | 68 | −74.73 | −99.04 | 1 | 1 | 1 | 1 | 0.5 | 4.5 | Yes |
| 31 | 650 | 29 | 1.15 | 107 | −75.07 | −99.54 | 0.5 | 1 | 1 | 1 | 0.5 | 4 | Yes |
| 32 | 750 | 31 | 1.07 | 141 | −74.03 | −98.83 | 0.5 | 0 | 0 | 1 | 0.5 | 2 | No |
| 33 | 950 | 26 | 1.17 | 126 | −74.21 | −100.19 | 1 | 1 | 1 | 0.5 | 0.5 | 4 | No |
| 34 | 900 | 30 | 1.14 | 159 | −74.51 | −99.94 | 1 | 0 | 1 | 0.5 | 0.5 | 3 | Yes |

(*Continued*)

**Table 2.** *Tabulation of subglacial cone coordinates, dimensions and volcanic-interpretation confidence factors (see Table 1)* *(Continued)*

| Number | Height (m) | Average diameter (km) | Elongation ratio | Volume (km³) | Latitude | Longitude | Volcano confidence factor | | | | | | Previously identified |
|---|---|---|---|---|---|---|---|---|---|---|---|---|---|
| | | | | | | | 1 | 2 | 3 | 4 | 5 | Sum | |
| 35 | 300 | 15.5 | 1.21 | 14 | −74.72 | −100.09 | 1 | 0 | 1 | 0.5 | 0.5 | 3 | No |
| 36 | 325 | 11.5 | 1.30 | 8 | −75.24 | −96.95 | 1 | 1 | 1 | 0.5 | 0.5 | 4 | No |
| 37 | 500 | 34 | 1.13 | 113 | −72.19 | −97.70 | 0 | 1 | 1 | 1 | 0.5 | 3.5 | Yes |
| 38 | 1025 | 40.5 | 1.19 | 330 | −72.54 | −97.61 | 0 | 0 | 0.5 | 1 | 0.5 | 2 | Yes |
| 39 | 400 | 20.5 | 1.16 | 33 | −72.51 | −98.38 | 0 | 1 | 1 | 1 | 0.5 | 3.5 | Yes |
| 40 | 525 | 28 | 1.15 | 81 | −72.42 | −99.23 | 0.5 | 1 | 1 | 1 | 0.5 | 4 | Yes |
| 41 | 325 | 20.5 | 1.16 | 27 | −72.47 | −99.94 | 0 | 1 | 1 | 1 | 0.5 | 3.5 | Yes |
| 42 | 550 | 33.5 | 1.16 | 121 | −72.32 | −101.07 | 0.5 | 1 | 1 | 0.5 | 0.5 | 3.5 | Yes |
| 43 | 225 | 11.5 | 1.30 | 6 | −73.87 | −103.30 | 0 | 0.5 | 1 | 1 | 0.5 | 3 | No |
| 44 | 675 | 26.5 | 1.12 | 93 | −75.45 | −103.29 | 1 | 1 | 1 | 0.5 | 1 | 4.5 | No |
| 45 | 350 | 9.5 | 1.38 | 6 | −78.41 | −101.96 | 1 | 0 | 0 | 0.5 | 0.5 | 2 | No |
| 46 | 575 | 23 | 1.19 | 60 | −79.65 | −101.80 | 1 | 0.5 | 0 | 1 | 0.5 | 3 | No |
| 47 | 275 | 12 | 1.18 | 8 | −80.03 | −101.60 | 1 | 0.5 | 0 | 0.5 | 0 | 2 | No |
| 48 | 250 | 13 | 1.17 | 8 | −80.15 | −101.46 | 1 | 0.5 | 0 | 0.5 | 0 | 2 | No |
| 49 | 175 | 21.5 | 1.15 | 16 | −80.17 | −103.39 | 0.5 | 0.5 | | 0.5 | 0.5 | 2 | No |
| 50 | 325 | 22 | 1.20 | 31 | −78.87 | −102.91 | 1 | 0.5 | 0.5 | 0.5 | 0 | 2.5 | No |
| 51 | 225 | 27 | 1.16 | 32 | −80.40 | −105.61 | 0.5 | 1 | 0 | 1 | 0.5 | 3 | No |
| 52 | 1175 | 23 | 1.19 | 122 | −78.74 | −104.24 | 1 | 1 | 1 | 0.5 | 1 | 4.5 | No |
| 53 | 125 | 15 | 1.14 | 6 | −77.61 | −103.56 | 1 | 0.5 | 0.5 | 0.5 | 1 | 3.5 | No |
| 54 | 225 | 11.5 | 1.30 | 6 | −82.05 | −111.42 | 1 | 0.5 | 1 | 1 | 0.5 | 4 | No |
| 55 | 175 | 23 | 1.19 | 18 | −77.43 | −105.77 | 1 | 1 | 1 | 1 | 0.5 | 4.5 | No |
| 56 | 150 | 9 | 1.25 | 2 | −77.70 | −74.55 | 1 | 0.5 | 0 | 0.5 | 0 | 2 | No |
| 57 | 275 | 13.5 | 1.25 | 10 | −78.46 | −107.77 | 1 | 0.5 | 1 | 0.5 | 0 | 3 | No |
| 58 | 175 | 11 | 1.44 | 4 | −76.72 | −106.61 | 1 | 1 | 1 | 1 | 0.5 | 4.5 | No |
| 59 | 150 | 12.5 | 1.27 | 5 | −76.87 | −106.38 | 1 | 1 | 1 | 1 | 1 | 5 | No |
| 60 | 1200 | 33.5 | 1.16 | 264 | −79.15 | −111.05 | 1 | 0 | 1 | 1 | 1 | 4 | No |
| 61 | 450 | 14.5 | 1.23 | 19 | −79.60 | −111.45 | 1 | 0 | 0 | 1 | 0.5 | 2.5 | No |
| 62 | 200 | 6 | 1.40 | 1 | −80.42 | −114.00 | 1 | 0.5 | 0 | 1 | 0 | 2.5 | No |
| 63 | 425 | 10 | 1.22 | 8 | −75.22 | −106.92 | 0 | 0.5 | 0.5 | 0.5 | 0.5 | 2 | No |
| 64 | 450 | 18 | 1.12 | 29 | −75.71 | −108.40 | 1 | 0 | 1 | 0.5 | 1 | 3.5 | No |
| 65 | 375 | 14.5 | 1.23 | 15 | −76.11 | −107.68 | 1 | 0 | 1 | 0.5 | 1 | 3.5 | No |
| 66 | 400 | 17 | 1.27 | 23 | −76.38 | −109.78 | 1 | 0.5 | 1 | 1 | 1 | 4.5 | No |
| 67 | 325 | 10.5 | 1.33 | 7 | −74.60 | −110.62 | 0.5 | 1 | 1 | 0.5 | 0.5 | 3.5 | No |
| 68 | 400 | 19 | 1.24 | 28 | −74.81 | −110.57 | 1 | 1 | 1 | 0.5 | 0.5 | 4 | No |
| 69 | 350 | 14 | 1.33 | 13 | −75.00 | −110.43 | 0.5 | 1 | 1 | 0.5 | 0.5 | 3.5 | No |
| 70 | 750 | 30 | 1.14 | 132 | −74.89 | −111.26 | 1 | 1 | 1 | 0.5 | 0.5 | 4 | No |
| 71 | 2300 | 51.5 | 1.15 | 1197 | −75.60 | −110.70 | 1 | 1 | 1 | 0.5 | 1 | 4.5 | Yes |

| | | | | | | | | | | | | | |
|---|---|---|---|---|---|---|---|---|---|---|---|---|---|
| 72 | 3200 | 58.5 | 1.13 | 2149 | −76.52 | −112.02 | 1 | 1 | 1 | 1 | 1 | 5 | Yes |
| 73 | 250 | 15.5 | 1.07 | 12 | −77.21 | −111.92 | 1 | 0 | 0.5 | 0.5 | 1 | 3 | No |
| 74 | 1025 | 36 | 1.00 | 261 | −77.72 | −112.64 | 1 | 0.5 | 1 | 1 | 0.5 | 4 | No |
| 75 | 300 | 16 | 1.13 | 15 | −77.67 | −114.04 | 1 | 0.5 | 1 | 0.5 | 1 | 4 | No |
| 76 | 625 | 26 | 1.17 | 83 | −77.80 | −115.00 | 1 | 1 | 1 | 0.5 | 1 | 4.5 | No |
| 77 | 650 | 12 | 1.18 | 18 | −78.08 | −115.37 | 1 | 0 | 0.5 | 0.5 | 0 | 2 | No |
| 78 | 400 | 10.5 | 1.33 | 9 | −78.11 | −115.93 | 1 | 1 | 0.5 | 0.5 | 0 | 3 | No |
| 79 | 350 | 13.5 | 1.25 | 13 | −78.93 | −115.69 | 1 | 0 | 0.5 | 1 | 1 | 3.5 | No |
| 80 | 325 | 20.5 | 1.28 | 27 | −79.68 | −113.53 | 1 | 1 | 0 | 1 | 1 | 4 | No |
| 81 | 200 | 6 | 1.40 | 1 | −80.38 | −115.11 | 1 | 0.5 | 0 | 1 | 1 | 3.5 | No |
| 82 | 125 | 4.5 | 1.25 | 0 | −80.38 | −115.11 | 1 | 0.5 | 0 | 1 | 1 | 3.5 | No |
| 83 | 150 | 10 | 1.22 | 3 | −80.34 | −116.40 | 1 | 1 | 0 | 1 | 1 | 4 | No |
| 84 | 1750 | 31.5 | 1.10 | 341 | −80.30 | −117.49 | 1 | 1 | 1 | 1 | 1 | 5 | No |
| 85 | 800 | 20 | 1.22 | 63 | −80.37 | −118.90 | 1 | 0.5 | 1 | 1 | 1 | 4.5 | No |
| 86 | 750 | 18.5 | 1.31 | 50 | −80.73 | −117.56 | 1 | 1 | 1 | 1 | 1 | 5 | No |
| 87 | 150 | 10.5 | 1.33 | 3 | −80.81 | −118.65 | 1 | 1 | 0 | 1 | 1 | 4 | No |
| 88 | 225 | 13 | 1.36 | 7 | −80.87 | −120.70 | 1 | 0 | 0 | 1 | 1 | 3 | No |
| 89 | 100 | 9 | 1.25 | 2 | −80.27 | −117.62 | 1 | 1 | 0 | 0 | 0 | 2 | No |
| 90 | 150 | 10.5 | 1.33 | 3 | −80.41 | −118.65 | 1 | 1 | 1 | 1 | 0.5 | 4.5 | No |
| 91 | 550 | 29.5 | 1.19 | 94 | −80.62 | −120.12 | 1 | 0.5 | 1 | 1 | 1 | 4.5 | No |
| 92 | 250 | 12.5 | 1.27 | 8 | −79.96 | −120.20 | 1 | 1 | 1 | 1 | 0.5 | 4.5 | No |
| 93 | 150 | 10 | 1.22 | 3 | −79.24 | −119.18 | 1 | 1 | 0 | 1 | 0 | 3 | No |
| 94 | 100 | 8 | 1.00 | 1 | −79.37 | −119.00 | 1 | 1 | 0 | 0 | 0 | 2 | No |
| 95 | 125 | 7.5 | 1.14 | 1 | −79.78 | −115.18 | 1 | 0 | 0 | 0.5 | 0.5 | 2 | No |
| 96 | 100 | 8.5 | 1.13 | 1 | −78.46 | −120.28 | 1 | 0 | 0.5 | 1 | 1 | 3.5 | No |
| 97 | 1000 | 28.5 | 1.19 | 159 | −77.54 | −118.28 | 0.5 | 1 | 0.5 | 0.5 | 0.5 | 3 | No |
| 98 | 2600 | 49.5 | 1.11 | 1250 | −76.96 | −117.78 | 1 | 1 | 1 | 0.5 | 1 | 4.5 | Yes |
| 99 | 3850 | 58 | 1.11 | 2542 | −76.07 | −115.94 | 0.5 | 1 | 1 | 1 | 1 | 4.5 | No |
| 100 | 1350 | 27.5 | 1.29 | 200 | −76.73 | −125.76 | 1 | 1 | 1 | 1 | 0.5 | 4.5 | Yes |
| 101 | 1100 | 21 | 1.21 | 95 | −76.93 | −125.73 | 1 | 1 | 1 | 1 | 0.5 | 4.5 | Yes |
| 102 | 1050 | 20 | 1.11 | 82 | −77.11 | −125.89 | 0.5 | 1 | 1 | 0.5 | 0.5 | 3.5 | Yes |
| 103 | 2400 | 39 | 1.17 | 716 | −77.32 | −125.97 | 1 | 1 | 1 | 0.5 | 0.5 | 4 | Yes |
| 104 | 1100 | 22 | 1.20 | 104 | −77.46 | −126.85 | 0.5 | 1 | 1 | 0.5 | 0.5 | 3.5 | Yes |
| 105 | 550 | 29 | 1.15 | 91 | −79.24 | −128.12 | 0.5 | 0 | 1 | 0.5 | 0.5 | 2.5 | No |
| 106 | 600 | 17 | 1.27 | 34 | −81.34 | −125.35 | 1 | 0.5 | 0 | 1 | 1 | 3.5 | No |
| 107 | 150 | 11.5 | 1.30 | 4 | −82.36 | −127.50 | 1 | 1 | 1 | 1 | 1 | 5 | No |
| 108 | 600 | 25.5 | 1.13 | 77 | −83.98 | −133.02 | 1 | 0 | 1 | 0.5 | 0.5 | 3 | No |
| 109 | 500 | 39 | 1.11 | 149 | −84.31 | −131.87 | 1 | 0.5 | 1 | 0.5 | 0.5 | 3.5 | No |
| 110 | 125 | 11.5 | 1.30 | 3 | −81.82 | −128.45 | 1 | 0.5 | 1 | 1 | 1 | 4.5 | No |
| 111 | 100 | 8 | 1.29 | 1 | −81.20 | −129.58 | 1 | 1 | 0 | 0 | 0 | 2 | No |
| 112 | 550 | 42 | 1.15 | 190 | −81.62 | −130.38 | 1 | 0 | 1 | 1 | 1 | 4 | No |

(*Continued*)

**Table 2.** *Tabulation of subglacial cone coordinates, dimensions and volcanic-interpretation confidence factors (see Table 1)* (*Continued*)

| Number | Height (m) | Average diameter (km) | Elongation ratio | Volume (km³) | Latitude | Longitude | Volcano confidence factor | | | | | | Previously identified |
|---|---|---|---|---|---|---|---|---|---|---|---|---|---|
| | | | | | | | 1 | 2 | 3 | 4 | 5 | Sum | |
| 113 | 275 | 28.5 | 1.19 | 44 | −81.87 | −130.76 | 1 | 0 | 0 | 1 | 1 | 3 | No |
| 114 | 350 | 29 | 1.07 | 58 | −82.41 | −134.85 | 1 | 1 | 1 | 0.5 | 0.5 | 4 | No |
| 115 | 150 | 10.5 | 1.33 | 3 | −81.10 | −132.52 | 1 | 0.5 | 1 | 1 | 1 | 4.5 | No |
| 116 | 400 | 31.5 | 1.25 | 78 | −81.36 | −133.60 | 1 | 1 | 1 | 0 | 0.5 | 3.5 | No |
| 117 | 100 | 6 | 1.40 | 1 | −81.64 | −134.55 | 1 | 0 | 0 | 0 | 1 | 2 | No |
| 118 | 250 | 15.5 | 1.07 | 12 | −81.55 | −135.48 | 1 | 0 | 1 | 1 | 0.5 | 3.5 | No |
| 119 | 550 | 21.5 | 1.15 | 50 | −80.35 | −131.14 | 1 | 1 | 1 | 0 | 1 | 4 | No |
| 120 | 250 | 11.5 | 1.30 | 6 | −80.50 | −134.03 | 1 | 0 | 1 | 1 | 1 | 4 | No |
| 121 | 950 | 36 | 1.12 | 242 | −80.23 | −134.29 | 1 | 0.5 | 1 | 1 | 0 | 3.5 | No |
| 122 | 250 | 30.5 | 1.03 | 46 | −79.57 | −132.88 | 1 | 0 | 0 | 0.5 | 0.5 | 2 | No |
| 123 | 325 | 23.5 | 1.24 | 35 | −80.40 | −136.32 | 0.5 | 0 | 1 | 1 | 1 | 3.5 | No |
| 124 | 400 | 29 | 1.00 | 66 | −80.08 | −138.89 | 0.5 | 0.5 | 0 | 1 | 0.5 | 2.5 | No |
| 125 | 275 | 32.5 | 1.10 | 57 | −79.39 | −137.82 | 0.5 | 0.5 | 1 | 1 | 0.5 | 3.5 | No |
| 126 | 125 | 17.5 | 1.19 | 8 | −79.67 | −138.15 | 0.5 | 0 | 1 | 0.5 | 0.5 | 2.5 | No |
| 127 | 250 | 19 | 1.11 | 18 | −79.76 | −139.69 | 1 | 0 | 0 | 0.5 | 0.5 | 2 | No |
| 128 | 400 | 24 | 1.18 | 45 | −78.70 | −137.18 | 0.5 | 1 | 0 | 0.5 | 0.5 | 2.5 | No |
| 129 | 300 | 10.5 | 1.33 | 6 | −78.61 | −137.87 | 0.5 | 0 | 1 | 0.5 | 0.5 | 2.5 | No |
| 130 | 600 | 25.5 | 1.13 | 77 | −78.39 | −139.25 | 1 | 0.5 | 1 | 1 | 0.5 | 4 | No |
| 131 | 425 | 39.5 | 1.08 | 130 | −79.00 | −142.10 | 1 | 0.5 | 0 | 0.5 | 0.5 | 2.5 | No |
| 132 | 700 | 31 | 1.00 | 132 | −78.15 | −140.91 | 1 | 0.5 | 1 | 0.5 | 0.5 | 3.5 | No |
| 133 | 675 | 22 | 1.00 | 64 | −77.91 | −140.89 | 1 | 1 | 1 | 0.5 | 0.5 | 4 | No |
| 134 | 2600 | 52.5 | 1.06 | 1406 | −73.71 | −126.54 | 0 | 1 | 1 | 1 | 0.5 | 3.5 | Yes |
| 135 | 400 | 28 | 1.15 | 62 | −74.69 | −127.78 | 0.5 | 1 | 1 | 0.5 | 0.5 | 3.5 | No |
| 136 | 200 | 4.5 | 1.25 | 1 | −75.98 | −128.21 | 0 | 1 | 1 | 1 | 0.5 | 3.5 | Yes |
| 137 | 1700 | 47.5 | 1.16 | 753 | −76.11 | −128.64 | 0 | 1 | 1 | 1 | 0.5 | 3.5 | No |
| 138 | 325 | 16 | 1.13 | 16 | −75.80 | −128.57 | 0 | 1 | 1 | 1 | 0.5 | 3.5 | No |
| 139 | 1500 | 19.5 | 1.17 | 112 | −75.98 | −129.11 | 0 | 1 | 1 | 1 | 0.5 | 3.5 | Yes |
| 140 | 450 | 5.5 | 1.20 | 3 | −75.90 | −129.29 | 0 | 1 | 1 | 1 | 0.5 | 3.5 | No |
| 141 | 1800 | 36 | 1.06 | 458 | −75.98 | −132.31 | 0.5 | 1 | 1 | 0.5 | 0.5 | 3.5 | Yes |
| 142 | 900 | 21 | 1.00 | 78 | −76.24 | −132.63 | 0.5 | 1 | 1 | 0.5 | 0.5 | 3.5 | Yes |
| 143 | 400 | 5 | 1.00 | 2 | −76.22 | −133.14 | 0 | 1 | 1 | 0.5 | 0.5 | 3 | No |
| 144 | 600 | 13 | 1.17 | 20 | −76.27 | −135.11 | 0 | 1 | 1 | 0.5 | 0.5 | 3 | Yes |
| 145 | 950 | 18.5 | 1.18 | 64 | −76.27 | −136.12 | 0 | 1 | 1 | 0.5 | 0.5 | 3 | Yes |
| 146 | 800 | 9.5 | 1.11 | 14 | −75.88 | −137.95 | 0 | 1 | 1 | 0.5 | 0.5 | 3 | No |
| 147 | 275 | 19.5 | 1.17 | 21 | −75.62 | −138.08 | 0 | 1 | 1 | 0.5 | 0.5 | 3 | No |
| 148 | 600 | 8.5 | 1.13 | 9 | −78.09 | −153.87 | 1 | 1 | 1 | 1 | 0.5 | 4.5 | No |
| 149 | 450 | 21.5 | 1.15 | 41 | −78.13 | −155.26 | 1 | 1 | 1 | 1 | 0.5 | 4.5 | No |

| | | | | | | | | | | | | | |
|---|---|---|---|---|---|---|---|---|---|---|---|---|---|
| 150 | 775 | 23 | 1.19 | 80 | −77.88 | −153.60 | 1 | 1 | 1 | 1 | 0.5 | 4.5 | No |
| 151 | 275 | 16.5 | 1.06 | 15 | −77.89 | −154.81 | 1 | 1 | 1 | 1 | 0.5 | 4.5 | No |
| 152 | 100 | 7 | 1.33 | 1 | −78.19 | −157.00 | 0 | 1 | 1 | 0.5 | 0.5 | 3 | No |
| 153 | 125 | 18 | 1.25 | 8 | −82.11 | −154.71 | 0 | 0 | 1 | 0.5 | 0.5 | 2 | No |
| 154 | 100 | 16.5 | 1.06 | 5 | −81.96 | −157.64 | 0 | 0 | 1 | 0.5 | 0.5 | 2 | No |
| 155 | 150 | 24 | 1.18 | 17 | −81.53 | −163.39 | 1 | 1 | 1 | 0.5 | 0.5 | 4 | No |
| 156 | 225 | 15 | 1.00 | 10 | −78.00 | −165.52 | 0 | 0.5 | 0.5 | 1 | 0.5 | 2.5 | No |
| 157 | 100 | 12 | 1.18 | 3 | −77.18 | −164.77 | 0 | 0.5 | 0.5 | 1 | 0.5 | 2.5 | No |
| 158 | 1400 | 34 | 1.13 | 318 | −85.96 | −163.98 | 0.5 | 1 | 1 | 0.5 | 0.5 | 3.5 | Yes |
| 159 | 400 | 10.5 | 1.33 | 9 | −78.39 | 167.56 | 0.5 | 1 | 1 | 1 | 0.5 | 4 | Yes |
| 160 | 325 | 16.5 | 1.20 | 17 | −78.50 | 166.04 | 0 | 1 | 1 | 1 | 0.5 | 3.5 | Yes |
| 161 | 1600 | 29 | 1.07 | 264 | −78.61 | 165.08 | 0 | 1 | 1 | 1 | 0.5 | 3.5 | Yes |
| 162 | 2050 | 39.5 | 1.14 | 628 | −78.73 | 163.67 | 0 | 1 | 1 | 1 | 0.5 | 3.5 | Yes |
| 163 | 2250 | 33 | 1.13 | 481 | −77.78 | 168.67 | 0 | 1 | 1 | 1 | 0.5 | 3.5 | Yes |
| 164 | 1800 | 29.5 | 1.19 | 307 | −77.70 | 166.83 | 0 | 1 | 1 | 1 | 0.5 | 3.5 | Yes |
| 165 | 1250 | 21 | 1.10 | 108 | −77.49 | 166.78 | 0 | 1 | 1 | 1 | 0.5 | 3.5 | Yes |
| 166 | 425 | 22.5 | 1.14 | 42 | −77.23 | 167.68 | 0 | 1 | 1 | 1 | 0.5 | 3.5 | Yes |
| 167 | 350 | 20.5 | 1.16 | 29 | −77.18 | 166.94 | 0 | 1 | 1 | 0.5 | 0.5 | 3 | Yes |
| 168 | 750 | 16.5 | 1.20 | 40 | −74.58 | 164.22 | 1 | 1 | 1 | 1 | 0.5 | 4.5 | Yes |
| 169 | 600 | 26.5 | 1.21 | 83 | −73.80 | 169.69 | 0.5 | 1 | 1 | 1 | 0.5 | 4 | Yes |
| 170 | 950 | 33.5 | 1.09 | 209 | −73.42 | 164.70 | 0 | 1 | 1 | 1 | 0.5 | 3.5 | Yes |
| 171 | 1550 | 34.5 | 1.16 | 362 | −72.78 | 169.89 | 0 | 1 | 1 | 0.5 | 0.5 | 3 | Yes |
| 172 | 750 | 17.5 | 1.19 | 45 | −71.93 | 170.41 | 0 | 1 | 1 | 1 | 0.5 | 3.5 | Yes |
| 173 | 500 | 25.5 | 1.13 | 64 | −76.45 | −165.16 | 0 | 0.5 | 0.5 | 0.5 | 0.5 | 2 | No |
| 174 | 450 | 34.5 | 1.09 | 105 | −76.37 | −166.16 | 0 | 0.5 | 0.5 | 0.5 | 0.5 | 2 | No |
| 175 | 450 | 13.5 | 1.25 | 16 | −76.12 | −72.41 | 0.5 | 1 | 1 | 1 | 0.5 | 4 | Yes |
| 176 | 400 | 9.5 | 1.38 | 7 | −73.68 | −78.91 | 0 | 1 | 1 | 0.5 | 0.5 | 3 | No |
| 177 | 550 | 20 | 1.22 | 43 | −73.70 | −79.43 | 0.5 | 1 | 1 | 1 | 0.5 | 4 | Yes |
| 178 | 300 | 17 | 1.27 | 17 | −74.67 | −78.72 | 0.5 | 1 | 1 | 1 | 0.5 | 4 | Yes |
| Average | 621 | 21.3 | 1.18 | 121 | −77.56 | −120.28 | 0.69 | 0.69 | 0.71 | 0.74 | 0.57 | 3.40 | |

The final column identifies whether the cone was a previously recognized volcano (Yes) or a new discovery (No). Most of the previously identified volcanoes are catalogued in LeMasurier *et al.* (1990).
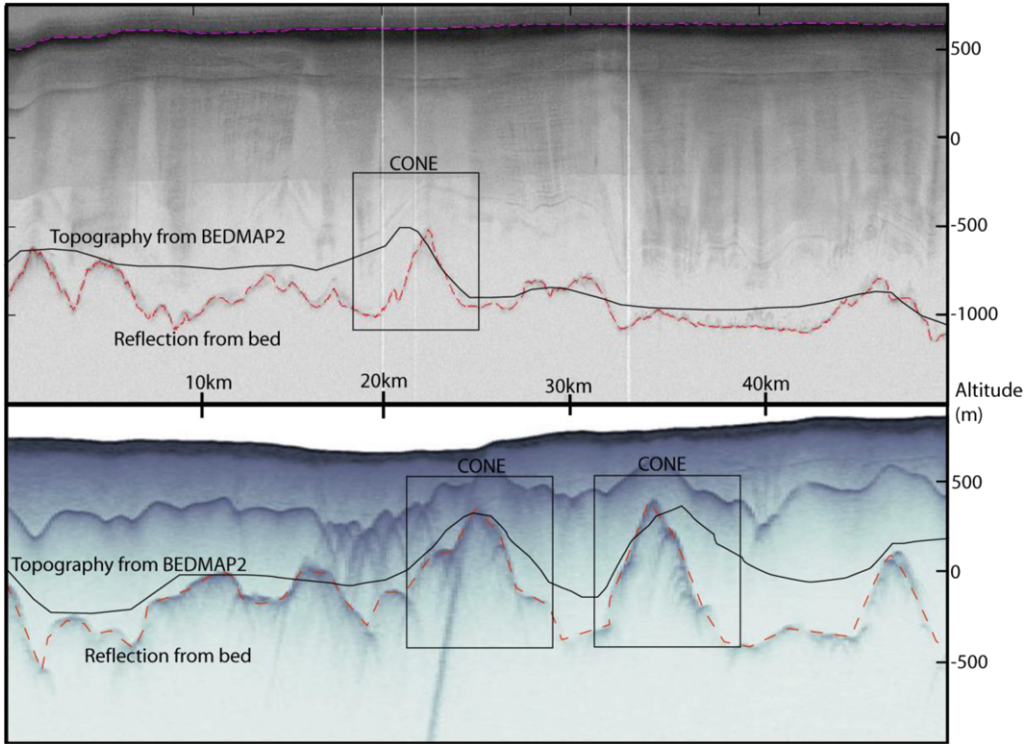
**Fig. 3.** The upper panel shows an echogram from NASA's Icebridge mission (NSIDC 2014) that shows generally good agreement between a cone on the echogram and on the Bedmap2 data. The lower panel shows an echogram from Corr & Vaughan (2008) with basal topography picking out two cones; the dark layer above the bed is tephra believed to have erupted around 2000 years ago.

unknown volcanic edifices across the ice-shrouded WARS.

### Extent and activity of subglacial volcanism

We have identified at least 138 likely volcanic edifices distributed throughout the WARS. This represents a significant advance on the total of 47 identified volcanoes across the whole of West Antarctica, most of which are visible at the surface and are situated in Marie Byrd Land and the Transantarctic Mountains (LeMasurier *et al.* 1990). The wide distribution of volcanic structures throughout the WARS, along with the presence of clusters of

**Table 3.** *Statistical comparison of the morphologies of the cones identified in this study identified as volcanoes*

|  | Height (m) | | Average diameter (km) | | Axis ratio | | Volume (km$^3$) | | Confidence factor |
|---|---|---|---|---|---|---|---|---|---|
|  | (a) | (b) | (a) | (b) | (a) | (b) | (a) | (b) | (a) |
| Average | 701 | 940 | 21.9 | 17.1 | 1.19 | 2.11 | 144 | 150 | 3.75 |
| Standard Deviation | 641 | 670 | 10.7 | 11.6 | 0.09 | 0.81 | 345 | 371 | 0.56 |
| Median | 475 | 810 | 20.5 | 15.3 | 1.17 | 1.98 | 42 | 31 | 3.5 |
| Minimum | 100 | 100 | 4.5 | 2.3 | 1.00 | 1.13 | 0.5 | 0.2 | 3 |
| Maximum | 3850 | 3030 | 58.5 | 63.3 | 1.44 | 5.23 | 2542 | 3086 | 5 |

Comparison with: (a) those from a global database of shield volcanoes; and (b) Grosse *et al.* (2014). The two are similar, apart from the long-short axis ratio; our cones are, on average, more circular than shield volcanoes elsewhere. This could be linked to specific glaciovolcanic eruption mechanisms, but is most likely a data bias due to our detection methods excluding more elliptical edifices.
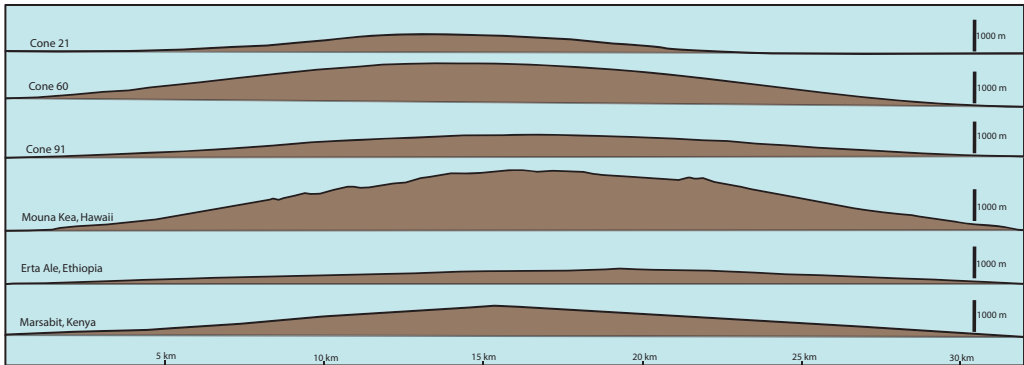
**Fig. 4.** Cross-sections of three cones from this study (numbers 21, 60 and 91: see Fig. 2 and Table 2 for more details and locations) and three prominent shield volcanoes, namely Mauna Kea (Hawaii), Erta Ale and Marsabit (East African Rift).

volcanism concentrated within the Marie Byrd Land dome, is markedly similar to the East African Rift System, which is also >2000 km in length and flanked by the Ethiopian and Kenyan domes (Fig. 1b) (Siebert & Simkin 2002; Ebinger 2005). Morphologically, the volcanoes have volume–height characteristics and basal diameters that closely match those of rift volcanoes around the world (Fig. 5; Table 3). Bearing in mind that data paucity beneath the Ross Ice Shelf precluded meaningful analysis of a significant terrain also considered to be part of the WARS, the total region that has experienced volcanism is likely to be considerably larger than that we have identified here.
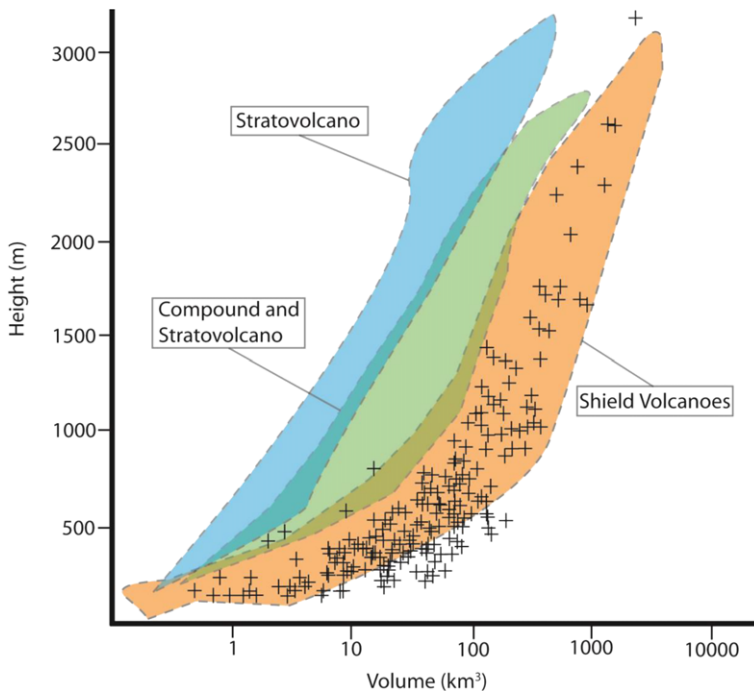


**Fig. 5.** Volume/height chart of the cones from this study (crosses) superimposed over data from volcanoes worldwide (Grosse *et al.* 2014). The cones closely fit the morphology data for shield volcanoes, as would be expected for basalt-dominated rift volcanism.

The activity of the WARS has been the subject of a longstanding debate, with one side advocating a largely inactive rift (LeMasurier 2008) and others suggesting large-scale volcanism (Behrendt *et al.* 2002). The arguments in favour of an inactive rift are based on the anomalously low elevation of the WARS compared to other active continental rifts (Winberry & Anandakrishnan 2004; LeMasurier 2008) and the relative absence of basalt pebbles recovered from boreholes (LeMasurier pers. comm. 2015). Conversely, high regional heat fluxes (Shapiro & Ritzwoller 2004; Schroeder *et al.* 2014), geomagnetic anomalies (Behrendt *et al.* 2002) and evidence of recent subglacial volcanism (Blankenship *et al.* 1993; Corr & Vaughan 2008) suggest that the rift is currently active. This study provides evidence of a large number of subglacial volcanoes, with their quasi-conical shield volcano type geometries still intact. The largely uneroded nature of the cones suggests that many may be of Pleistocene age or younger, which supports the argument that the rift remains active today.

From this study, we are not able to determine whether the different volcanoes are active or not; however, the identification of multiple new volcanic edifices, and the improved regional sense of their geographical spread and concentration across the WARS, may guide future investigation of their activity. Several previous studies have suggested that the Marie Byrd Land massif is supported by particularly low-density mantle, possibly comprising a volcanic 'hotspot' (Hole & LeMasurier 1994; Winberry & Anandakrishnan 2004). Tephra layers recovered from the Byrd Ice Core near the WAIS divide suggest that multiple Marie Byrd Land volcanoes were active in the Late Quaternary (Wilch *et al.* 1999), while recent seismic activity in Marie Byrd Land has been interpreted as currently active volcanism (Lough *et al.* 2013). In the Pine Island Glacier catchment, strong radar-sounded englacial reflectors have been interpreted as evidence of a local eruption that occurred approximately 2000–2400 years ago (Fig. 3) (see Corr & Vaughan 2008) while, on the opposite rift flank in the Transantarctic Mountains, Mount Erebus comprises a known active volcano located above another potential volcanic hotspot (Gupta *et al.* 2009). Volcanism across the region is also likely to contribute to the elevated geothermal heat fluxes that have been inferred to underlie much of the WAIS (Shapiro & Ritzwoller 2004; Fox Maule *et al.* 2005; Schroeder *et al.* 2014). The deployment of broadband seismics to recover the mantle structure beneath the WAIS is now showing great promise (e.g. Heeszel *et al.* 2016), and our map of potential volcanic locations could help target further installations directed towards improved monitoring of the continent's subglacial volcanic activity.

## Implications for ice stability and future volcanism

The wide spread of volcanic edifices and the possibility of extensive volcanism throughout the WARS also provides potential influences on the stability of the WAIS. Many parts of the WAIS overlie basins that descend from sea level with distance inland, lending the ice sheet a geometry that is prone to runaway retreat (Bamber *et al.* 2009; Alley *et al.* 2015). Geological evidence points to the likelihood that the WAIS experienced extensive retreat during Quaternary glacial minima (Naish *et al.* 2009) and concurrently contributed several metres to global sea-level rise (O'Leary *et al.* 2013). Currently, the WAIS may be undergoing another such wholesale retreat, as ice in the Pacific-facing sector has consistently been retreating from the time of the earliest aerial and satellite observations (Rignot 2002; McMillan *et al.* 2014; Mouginot *et al.* 2014). We do not consider it likely that volcanism has played a significant role in triggering the current retreat, for which there is compelling evidence that the forcing has initiated from the margins (Turner *et al.* 2017), but we do propose that subglacial volcanism has the potential to influence future rates of retreat by (1) producing enhanced basal melting that could impact upon basal ice motion and (2) providing edifices that may act to pin retreat.

On the first of these possibilities, some authors have suggested that active subglacial volcanism, through providing enhanced basal melting that might 'lubricate' basal motion, could play a role in WAIS instability (Blankenship *et al.* 1993; Vogel *et al.* 2006; Corr & Vaughan 2008). A possible analogy is provided by subglacial volcanism in Iceland, where subglacial eruptions have been known to melt basal ice, flood the basal interface and induce periods of enhanced ice flow (e.g. Magnússon *et al.* 2007; Einarsson *et al.* 2016); however, in Iceland's ice caps the ice is considerably thinner than in the WAIS and, hence, more prone to subglacial-melt-induced uplift. Nevertheless, there is evidence to suggest that changes to subglacial water distribution can occur beneath the WAIS, and that they can sometimes have profound impacts on ice dynamics: examples are ice-dynamic variability over subglacial lakes (e.g. Siegfried *et al.* 2016) or the suggestion that subglacial water pulses may have been responsible for historical occurrences of ice-stream piracy (e.g. Anandakrishnan & Alley 1997; Vaughan *et al.* 2008). Much recent attention has focused on the drainage of subglacial lakes comprising plausible triggers of such dynamic changes, but subglacial eruptions may represent another pulsed-water source whose occurrence has rarely, if ever, been factored into ice-sheet models. Even inactive or dormant

volcanism has the potential to influence ice flow by increasing heat flux to the subglacial interface; this may generate a basal melt cavity and enhance ice flow (Bourgeois *et al.* 2000; Schroeder *et al.* 2014).

On the other hand, volcanic edifices, whether active or not, stand as significant protuberances which may act geometrically as stabilizing influences on ice retreat. Numerical models used to project potential rates of WAIS retreat show that, once initiated, ice retreat will continue unabated as long as the ice bed is smooth and downslopes inland, but that any increase in roughness or obstacle in the bed can act to delay or stem retreat (Ritz *et al.* 2015; Nias *et al.* 2016). We have identified here a number of volcanic edifices sitting within the WAIS' deep basins; these edifices, which are likely to owe their existence to volcanism, could represent some of the most influential pinning points for past and future ice retreat.

Looking ahead, the thinning and potential removal of ice cover from the WARS volcanic province could have profound impacts for future volcanic activity across the region. Research in Iceland has shown that with thinning ice cover, magma production has increased at depth as a response to decompression of the underlying mantle (Jull & McKenzie 1996; Schmidt *et al.* 2013). Moreover, there is evidence that, worldwide, volcanism is most frequent in deglaciating regions as the overburden pressure of the ice is first reduced and then removed (Huybers & Langmuir 2009; Praetorius *et al.* 2016). Unloading of the WAIS from the WARS therefore offers significant potential to increase partial melting and eruption rates throughout the rifted terrain. Indeed, the concentration of volcanic edifices along the WARS could be construed as evidence that such enhanced volcanic activity was a feature of Quaternary minima. This raises the possibility that in a future of thinning ice cover and glacial unloading over the WARS, subglacial volcanic activity may increase and this, in turn, may lead to enhanced water production and contribute to further potential ice-dynamical instability.

## Conclusions

By applying morphometric analysis to a digital elevation model of the West Antarctic Rift System, and assessing the results with respect to auxiliary information from ice-surface expressions to aerogeophysical data, we have identified 138 subglacial volcanic edifices spread throughout the rift. The volcanoes are widely distributed in the broad rift zone, with particular concentrations in Marie Byrd Land and along the central WARS axis. The results demonstrate that the West Antarctic Ice Sheet shrouds one of the world's largest volcanic

provinces, similar in scale to the East African Rift System. The overall volcano density beneath West Antarctica was found to be one edifice per $18\,500 \pm 500$ km$^2$, with a central belt along the rift's central sinuous ridge containing one edifice per $7800 \pm 400$ km$^2$. The presence of such a volcanic belt traversing the deepest marine basins beneath the centre of the West Antarctic Ice Sheet could prove to be a major influence on the past behaviour and future stability of the ice sheet.

## References

ALLEY, R.B., ANANDAKRISHNAN, S. *ET AL.* 2015. Oceanic forcing of ice sheet retreat: West Antarctica and more. *Annual Reviews in Earth and Planetary Sciences*, **43**, 207–231.

ANANDAKRISHNAN, S. & ALLEY, R.B. 1997. Stagnation of ice stream C, West Antarctica by water piracy. *Geophysical Research Letters*, **24**, 265–268.

BAMBER, J.L., RIVA, R.E.M., VERMEERSEN, B.L.A. & LE BROCQ, A.M. 2009. Reassessment of the potential sea-level rise from a collapse of the West Antarctic Ice Sheet. *Science*, **324**, 901–903.

BEHRENDT, J.C., LEMASURIER, W.E., COOPER, A.K., TESSENSOHN, F., TREHU, A. & DAMASKE, D. 1991. Geophysical studies of the West Antarctic Rift System. *Tectonics*, **10**, 1257–1273.

BEHRENDT, J.C., FINN, C.A., BLANKENSHIP, D.D. & BELL, R.E. 1998. Aeromagnetic evidence for a volcanic caldera(?) complex beneath the divide of the West Antarctic Ice Sheet. *Geophysical Research Letters*, **25**, 4385–4388.

BEHRENDT, J.C., BLANKENSHIP, D.D., MORSE, D.L., FINN, C.A. & BELL, R.E. 2002. Subglacial volcanic features beneath the West Antarctic Ice Sheet interpreted from aeromagnetic and radar ice sounding. *In*: SMELLIE, J.L. & CHAPMAN, M.G. (eds) *Volcano–Ice Interaction on Earth and Mars*. Geological Society, London, Special Publications, **202**, 337–355, https://doi.org/10.1144/GSL.SP.2002.202.01.17

BINGHAM, R.G. & SIEGERT, M.J. 2009. Quantifying subglacial bed roughness in Antarctica: implications for ice-sheet dynamics and history. *Quaternary Science Reviews*, **28**, 223–236.

BINGHAM, R.G., FERRACCIOLI, F., KING, E.C., LARTER, R.D., PRITCHARD, H.D., SMITH, A.M. & VAUGHAN, D.G. 2012. Inland thinning of West Antarctic Ice Sheet steered along subglacial rifts. *Nature*, **487**, 468–471.

BLANKENSHIP, D.D., BROZENA, R.B., BEHRENDT, J.C. & FINN, C.A. 1993. Active volcanism beneath the West Antarctic ice sheet and implications for ice-sheet stability. *Nature*, **361**, 526–529.

BO, S., SIEGERT, M.J. *ET AL.* 2009. The Gamburtsev mountains and the origin and early evolution of the Antarctic Ice Sheet. *Nature*, **459**, 690–693.

BOURGEOIS, O., DAUTEUIL, O. & VLIET-LANOE, B.V. 2000. Geothermal control on flow patterns in the Last Glacial

Maximum ice sheet of Iceland. *Earth Surface Processes and Landforms*, **25**, 59–76.

BROZ, P., HAUBER, E., PLATZ, T. & BALME, M. 2015. Evidence for Amazonian highly viscous lavas in the southern highlands on Mars. *Earth and Planetary Science Letters*, **415**, 200–212.

CHANG, M., JAMIESON, S.S.R., BENTLEY, M.J. & STOKES, C.R. 2015. The surficial and subglacial geomorphology of western Dronning Maud Land, Antarctica. *Journal of Maps*, **12**, 892–903.

CORR, H.F.J. & VAUGHAN, D.G. 2008. A recent volcanic eruption beneath the West Antarctic ice sheet. *Nature Geoscience*, **1**, 122–125.

DALZIEL, I.W.D. 2006. On the extent of the active West Antarctic Rift System. *Terra Antartica Reports*, **12**, 193–202.

DAMIANI, T.M., JORDAN, T.A., FERRACCIOLI, F., YOUNG, D.A. & BLANKENSHIP, D.D. 2014. Variable crustal thickness beneath Thwaites Glacier revealed from airborne gravimetry, possible implications for geothermal heat flux in West Antarctica. *Earth and Planetary Science Letters*, **407**, 109–122.

DE RYDT, J., GUDMUNDSSON, G.H., CORR, H.F.J. & CHRISTOFFERSEN, P. 2013. Surface undulations of Antarctic ice streams tightly controlled by bedrock topography. *The Cryosphere*, **7**, 407–417.

EBINGER, C.J. 2005. Continental break-up: the East African perspective. *Astronomical Geophysics*, **46**, 216–221.

EBINGER, C., AYELE, A. *ET AL.* 2010. Length and timescales of rift faulting and magma intrusion: the Afar Rifting cycle from 2005 to present. *Annual Review of Earth and Planetary Sciences*, **38**, 437–464.

EBINGER, C.J., VAN WIJK, J. & KEIR, D. 2013. The time scales of continental rifting: implications for global processes. *In*: BICKFORD, M.E. (ed.) *The Web of Geological Sciences: Advances, Impacts, and Interactions*. Geological Society of America, Special Papers, **500**, 371–396.

EINARSSON, B., MAGNÚSSON, E., ROBERTS, M.J., PÁLSSON, F., THORSTEINSSON, T. & JÓHANNSSON, T. 2016. A spectrum of jökulhlaup dynamics revealed by GPS measurements. *Annals of Glaciology*, **57**, 47–61.

ELLIOTT, D.H. 2013. The geological and tectonic evolution of the Transantarctic Mountains: a review. *In*: HAMBREY, M.J., BARKER, P.F., BARRETT, P.J., BOWMAN, V., DAVIES, B., SMELLIE, J.L. & TRANTER, M. (eds) *Antarctic Palaeoenvironments and Earth-Surface Processes*. Geological Society, London, Special Publications, **381**, 7–35, https://doi.org/10.1144/SP381.14

ELLIS, M. & KING, G. 1991. Structural control of flank volcanism in continental rifts. *Science*, **254**, 839–842.

ELY, J.C., CLARK, C.D. *ET AL.* 2016. Do subglacial bedforms comprise a size and shape continuum? *Geomorphology*, **257**, 108–119.

FAVALLI, M., KARÁTSON, D., YEPES, J. & NANNIPIERI, L. 2014. Surface fitting in geomorphology – examples for regular-shaped volcanic landforms. *Geomorphology*, **221**, 139–149.

FITZGERALD, P.G. 2002. Tectonics and landscape evolution of the Antarctic plate since the breakup of Gondwana, with an emphasis on the West Antarctic Rift System and the Transantarctic Mountains. *Royal Society of New Zealand Bulletin*, **35**, 453–469.

FOX MAULE, C., PURUCKER, M., OLSEN, N. & MOSEGAARD, K. 2005. Heat flux anomalies in Antarctica revealed from satellite magnetic data. *Science*, **309**, 464–467.

FRETWELL, P., PRITCHARD, H.D. *ET AL.* 2013. Bedmap2: improved ice bed, surface and thickness datasets for Antarctica. *The Cryosphere*, **7**, 375–393.

GLOBAL VOLCANISM PROGRAM 2013. VENZKE, E. (ed.) *Volcanoes of the World, v. 4.5.3*. Smithsonian Institution, https://doi.org/10.5479/si.GVP.VOTW4-2013

GROSSE, P., EUILLADES, P.A., EUILLADES, L.D. & VAN WYK DE VRIES, B. 2014. A global database of composite volcano morphology. *Bulletin of Volcanology*, **76**, 784.

GUPTA, S., ZHAO, D. & RAI, S.S. 2009. Seismic imaging of the upper mantle under the Erebus hotspot in Antarctica. *Gondwana Research*, **16**, 109–118.

HEESZEL, D.S., WIENS, D.A. *ET AL.* 2016. Upper mantle structure of central and West Antarctica from array analysis of Rayleigh wave phase velocities. *Journal of Geophysical Research*, **121**, 1758–1775.

HICKSON, C.J. 2000. Physical controls and resulting morphological forms of Quaternary ice-contact volcanoes in western Canada. *Geomorphology*, **32**, 239–261.

HOLE, M.J. & LEMASURIER, W.E. 1994. Tectonic controls on the geochemical composition of the Cenozoic, mafic volcanic alkaline rocks from West Antarctica. *Contributions to Mineralogy and Petrology*, **117**, 182–202.

HUYBERS, P. & LANGMUIR, C. 2009. Feedback between deglaciation, volcanism, and atmospheric $CO_2$. *Earth and Planetary Science Letters*, **286**, 479–491.

JAMIESON, S.S.R., SUGDEN, D.E. & HULTON, N.R.J. 2010. The evolution of the subglacial landscape of Antarctica. *Earth and Planetary Science Letters*, **293**, 1–27.

JAMIESON, S.S.R., STOKES, C.R. *ET AL.* 2014. The glacial geomorphology of the Antarctic ice sheet bed. *Antarctic Science*, **26**, 724–741.

JAMIESON, S.S.R., ROSS, N. *ET AL.* 2016. An extensive subglacial lake and canyon system in Princess Elizabeth Land, East Antarctica. *Geology*, **44**, 87–90.

JORDAN, T.A., FERRACCIOLI, F., VAUGHAN, D.G., HOLT, J.W., CORR, H., BLANKENSHIP, D.D. & DIEHL, T.M. 2010. Aerogravity evidence for major crustal thinning under the Pine Island Glacier region (West Antarctica). *Geological Society of America Bulletin*, **122**, 714–726.

JULL, M. & MCKENZIE, D. 1996. The effect of deglaciation on mantle melting beneath Iceland. *Journal of Geophysical Research*, **101**, 21815–21828.

KALBERG, T., GOHL, K., EAGLES, G. & SPIEGEL, C. 2015. Rift processes and crustal structure of the Amundsen Sea Embayment, West Antarctica, from 3D potential field modelling. *Marine Geophysical Research*, **36**, 263–279.

KIM, H.R., VON FRESE, R.R.B., TAYLOR, P.T., GOLYNSKY, A.V., GAYA-PIQUÉ, L.R. & FERRACCIOLI, F. 2007. Improved magnetic anomalies of the Antarctic lithosphere from satellite and near-surface data. *Geophysical Journal International*, **171**, 119–126.

LEMASURIER, W.E. 2008. Neogene extension and basin deepening in the West Antarctic rift inferred from comparisons with the East African rift and other analogs. *Geology*, **36**, 247–250.

LEMASURIER, W.E. 2013. Shield volcanoes of Marie Byrd Land, West Antarctic rift: oceanic island similarities, continental signature, and tectonic controls. *Bulletin of Volcanology*, **75**, 726.

LEMASURIER, W.E., THOMSON, J.W., BAKER, P.E., KYLE, P.R., ROWLEY, P.D., SMELLIE, J.L. & VERWOERD, W.J.

1990. *Volcanoes of the Antarctic Plate and Southern Oceans Antarctic*. American Geophysical Union, Antarctic Research Series, **48**.

LINDBACK, K. & PETTERSSON, R. 2015. Spectral roughness and glacial erosion of a land-terminating section of the Greenland Ice Sheet. *Geomorphology*, **238**, 149–159.

LOUGH, A.C. & OTHERS. 2013. Seismic detection of an active subglacial magmatic complex in Marie Byrd Land, Antarctica. *Nature Geoscience*, **6**, 1031–1035.

MAGNÚSSON, E., ROTT, H., BJÖRNSSON, H. & PÁLSSON, F. 2007. The impact of jökulhlaups on basal sliding observed by SAR interferometry on Vatnajökull, Iceland. *Journal of Glaciology*, **53**, 232–240.

McKNIGHT, S.B. & WILLIAMS, S.N. 1997. Old cinder cone or young composite volcano?: The nature of Cerro Negro, Nicaragua. *Geology*, **25**, 339–342.

McMILLAN, M., SHEPHERD, A. ET AL. 2014. Increased ice losses from Antarctica detected by CryoSat-2. *Geophysical Research Letters*, **41**, 3899–3905.

MOUGINOT, J., RIGNOT, E. & SCHEUCHL, B. 2014. Sustained increase in ice discharge from the Amundsen Sea Embayment, West Antarctica, from 1973 to 2013. *Geophysical Research Letters*, **41**, 1576–1584.

NAISH, T., POWELL, R. ET AL. 2009. Obliquity-paced Pliocene West Antarctic ice sheet oscillations. *Nature*, **458**, 322–328.

NIAS, I.J., CORNFORD, S.L. & PAYNE, A.J. 2016. Contrasting the modelled sensitivity of the Amundsen Sea Embayment ice streams. *Journal of Glaciology*, **62**, 552–562.

NSIDC 2014. *IceBridge Accumulation Radar L1B Geolocated Radar Echo Strength Profiles. Version 2, IRMCR1B*. NASA National Snow and Ice Data Center, Distributed Active Archive Center, Boulder CO, USA (updated 2015).

O'LEARY, M.J., HEARTY, P.J., THOMPSON, W.G., RAYMO, M.E., MITROVICA, J.X. & WEBSTER, J.M. 2013. Ice sheet collapse following a prolonged period of stable sea level during the last interglacial. *Nature Geoscience*, **6**, 796–800.

PEDERSEN, G.B.M. & GROSSE, P. 2014. Morphometry of subaerial shield volcanoes and glaciovolcanoes from Reykjanes Peninsula, Iceland: effects of eruption environment. *Journal of Volcanology and Geothermal Research*, **282**, 115–133.

POLLARD, D. & DeCONTO, R.M. 2009. Modelling West Antarctic ice sheet growth and collapse through the past five million years. *Nature*, **458**, 329–332.

PRAETORIUS, S., MIX, A. ET AL. 2016. Interaction between climate, volcanism, and isostatic rebound in Southeast Alaska during the last deglaciation. *Earth and Planetary Science Letters*, **452**, 79–89.

RIGNOT, E. 2002. Ice-shelf changes in Pine Island Bay, Antarctica, 1947–2000. *Journal of Glaciology*, **48**, 247–256.

RIGNOT, E., MOUGINOT, J. & SCHEUCHL, B. 2011. Ice flow of the Antarctic Ice Sheet. *Science*, **333**, 1427–1430.

RITZ, C., EDWARDS, T.L., DURAND, G., PAYNE, A.J., PEYAUD, V. & HINDMARSH, R.C.A. 2015. Potential sea-level rise from Antarctic ice-sheet instability constrained by observations. *Nature*, **528**, 115–118.

ROSE, K.C., FERRACCIOLI, F. ET AL. 2013. Early East Antarctic Ice Sheet growth recorded in the landscape of the Gamburtsev Subglacial Mountains. *Earth and Planetary Science Letters*, **375**, 1–12.

ROSE, K.C., ROSS, N. ET AL. 2014. A temperate former West Antarctic ice sheet suggested by an extensive zone of subglacial meltwater channels. *Geology*, **42**, 971–974.

ROSS, N., JORDAN, T.A. ET AL. 2014. The Ellsworth subglacial highlands: inception and retreat of the West Antarctic Ice Sheet. *Geological Society of America Bulletin*, **126**, 3–15.

SCAMBOS, T., HARAN, T., FAHNESTOCK, M., PAINTER, T. & BOHLANDER, J. 2007. MODIS-based Mosaic of Antarctica (MOA) data sets: Continent-wide surface morphology and snow grain size. *Remote Sensing of Environment*, **111**, 242–257.

SCHEINERT, M., FERRACCIOLI, F. ET AL. 2016. New Antarctic gravity anomaly grid for enhanced geodetic and geophysical studies in Antarctica. *Geophysical Research Letters*, **43**, 600–610.

SCHMIDT, P., LUND, B., HIERONYMUS, C., MACLENNAN, J., ÁRNARDÓTTIR, T. & PAGLI, C. 2013. Effects of present day deglaciation in Iceland on mantle melt production rates. *Journal of Geophysical Research*, **118**, 3366–3379.

SCHROEDER, D.M., BLANKENSHIP, D.D., YOUNG, D.A. & QUARTINI, E. 2014. Evidence for elevated and spatially variable geothermal flux beneath the West Antarctic Ice Sheet. *Proceedings of the National Academy of Sciences of the United States of America*, **111**, 9070–9072.

SHAPIRO, N.M. & RITZWOLLER, M.H. 2004. Inferring surface heat flux distributions guided by a global seismic model: particular application to Antarctica. *Earth and Planetary Science Letters*, **223**, 213–224.

SIDDOWAY, C.S. 2008. Tectonics of the West Antarctic rift system: new light on the history and dynamics of distributed intracontinental extension. *In*: COOPER, A.K., BARRETT, P.J., STAGG, H., STOREY, B., STUMP, E. & WISE, W. (eds) *Antarctica: A Keystone in a Changing World, Proceedings of the 10th International Symposium on Antarctic Earth Sciences*. The National Academies Press, Washington, DC, 91–114.

SIEBERT, L. & SIMKIN, T. 2002. *Volcanoes of the World: an Illustrated Catalog of Holocene Volcanoes and their Eruptions*. Smithsonian Institution, Global Volcanism Program Digital Information Series, **GVP-3**.

SIEGFRIED, M.R., FRICKER, H.A., CARTER, S.P. & TULACZYK, S. 2016. Episodic ice velocity fluctuations triggered by a subglacial flood in West Antarctica. *Geophysical Research Letters*, **43**, 2640–2648.

SMELLIE, J.L. 2008. Basaltic subglacial sheet-like sequences: Evidence for two types with different implications for the inferred thickness of associated ice. *Earth-Science Reviews*, **88**, 60–88.

SMELLIE, J.L. & EDWARDS, B.R. 2016. *Glaciovolcanism on Earth and Mars*. Cambridge University Press, Cambridge.

SPIEGEL, C., LINDOW, J. ET AL. 2016. Tectonomorphic evolution of Marie Byrd Land – Implications for Cenozoic rifting activity and onset of West Antarctic glaciation. *Global and Planetary Change*, **145**, 98–115.

STRETCH, R.C., MITCHELL, N.C. & PORTARO, R.A. 2006. A morphometric analysis of the submarine volcanic ridge south-east of Pico Island, Azores. *Journal of Volcanology and Geothermal Research*, **156**, 1–2, 35–54.

STUDINGER, M., BELL, R.E., BLANKENSHIP, D.D., FINN, C.A., ARKO, R.A., MORSE, D.L. & JOUGHIN, I. 2001.

Subglacial sediments: a regional geologic template for ice flow in West Antarctica. *Geophysical Research Letters*, **28**, 3493–3496.

STUDINGER, M., BELL, R.E., FINN, C.A. & BLANKENSHIP, D.D. 2002. Mesozoic and Cenozoic extensional tectonics of the West Antarctic Rift System from high-resolution airborne geophysical mapping. *Royal Society of New Zealand Bulletin*, **35**, 563–569.

TURNER, J., ORR, A., GUDMUNDSSON, G.H., JENKINS, A., BINGHAM, R.G., HILLENBRAND, C.-D. & BRACEGIRDLE, T.J. 2017. Atmosphere-ice-ocean interactions in the Amundsen Sea Embayment, West Antarctica. *Reviews of Geophysics*, **55**, 235–276.

VAUGHAN, D.G., CORR, H.F.J., SMITH, A.M., PRITCHARD, H. D. & SHEPHERD, A. 2008. Flow-switching and water piracy between Rutford Ice Stream and Carlson Inlet, West Antarctica. *Journal of Glaciology*, **54**, 41–48.

VOGEL, S.W., TULACZYK, S., CARTER, S., RENNE, P., TURRIN, B. & GRUNOW, A. 2006. Geologic constraints on the existence and distribution of West Antarctic subglacial volcanism. *Geophysical Research Letters*, **33**, L23501.

WARDELL, L.J., KYLE, P.R. & CHAFFIN, C. 2014. Carbon dioxide and carbon monoxide emission rates from an alkaline intra-plate volcano: Mt. Erebus, Antarctica. *Journal of Volcanology and Geothermal Research*, **131**, 109–121.

WILCH, T.I., MCINTOSH, W.C. & DUNBAR, N.W. 1999. Late Quaternary volcanic activity in Marie Byrd Land: potential $^{40}$Ar/$^{39}$Ar-dated time horizons in West Antarctic ice and marine cores. *Geological Society of America Bulletin*, **111**, 1563–1580.

WINBERRY, J.P. & ANANDAKRISHNAN, S. 2004. Crustal structure of the West Antarctic Rift System and Marie Byrd Land hotspot. *Geology*, **32**, 977–980.

YOUNG, D.A. & OTHERS. 2011. A dynamic early East Antarctic Ice Sheet suggested by ice-covered fjord landscapes. *Nature*, **474**, 72–75.